Tuijin Jishu/Journal of Propulsion Technology
ISSN: 1001-4055
Vol. 45 No. 4 (2024)

Experimental investigations for suitability of 3D Printed PLA and SS316L as a substitute for bone & bone interface in biomedical application

Akshay S Karad[a], Ratnakar R Ghorpade[a], Puskaraj D Sonawwanay[a*], Shivprkash B Barve[a]

[a] *Department of Mechanical Engineering, Dr. Vishwanath Karad MIT World Peace University, Pune, India*

Abstract:- This article focuses on using common and non-professional 3D printing hardware and software to create and test PLA polymer and Stainless Steel 316L cylindrical shell constructions. The former is manufactured using FDM technology, employing an equilateral grid pattern with 80% infill for solid which closely mimic bone and bone interface. CATIA V5 is used to generate parametric and automated 3D model for these constructions. Compressive structural strength and stiffness are two important factors in biomedical use. Porosity is consider 80% while the sample Modelling, Manufacturing and Testing the structure has been carried at lab UTM. The intrinsic limits of 3D printing, such as the anisotropic temperament of FDM, in-homogeneities, flaws, along with the impact of configurations on local buckling behaviour, are inferred from the experimental data. The experimental outcome demonstrates that SS 316L is strongest in compression (2249.42MPa) as compared to Solid PLA specimen with 80 infill (29.77MPa). Hollow polymer PLA specimen showed medium compressive strength (34.29 MPa experimentally. Static structural FEA simulation results were found to be within 10% range of the experimental results, and thus validation was achieved. The experimental tests showed that load carrying capacities of SS 316L, solid PLA with 80% infill and hollow PLA are 176580 N, 2066N and 1508N respectively. SEM is used to study morphology and possible prediction of failure of sample. It is concluded that hollow PLA material is the choice and substitute for bone and bone interface in biomedical applications considering its favourable properties determine experimentally in this work.

Keywords: *3D printing, PLA, SS316L*

1. Introduction

Basis of Literature Review

Various reputed databases of research and review articles such as Springer, Elsevier, MDPI, IEEE, Willey Online, etc. are referred to while performing the literature review. Initially we identified around 150 research articles and review articles to obtain specific information from the same. Subsequently we filtered these articles according to years (2015 to 2021).

2. Literature Review

Large surgical bone defects can be caused by various disorders, which include of trauma, malignancy, or infection. These abnormalities pose significant obstacles for reconstructive orthopaedic surgery. Currently available therapies include ceramic and acrylic bone cements, as well as autologous and allogenic bone grafting (1-2). These kinds of therapy have a number of disadvantages. Autografts cause morbidity at the donor site and pose a supply issue (3-5). While ceramic cements can aid in bone healing but are not as strong mechanically as acrylic cements, they do offer mechanical support without any regenerative qualities (6). Better bone substitutes that have the ability to regenerate tissue and offer mechanical support are therefore clinically needed but currently unmet.

Research on scaffolds composed of composite materials and polymers has been concentrated in this respect (3, 7). A developing field of study in bone healing is called tissue engineering (TE), in which scaffolds are coupled with cells and biologics to create momentary grafts that encourage tissue ingrowth and bone regeneration (8-13). With the long-standing objective of substituting impaired tissues and organs (14), TE seeks to preserve, enhance, or restore tissue functionality (2, 10). It is offered as a substitute strategy to get rid of the problems with allogeneic and autologous bone grafts (3, 15). Over time, various scaffolds have been developed for use in bone repair (57). To accomplish structural biomimicry, scaffolds must be necessarily fabricated as a permutation of materials (16-17) since bone tissue, which is made of organic components like collagen and the mineral hydroxyapatite, is a heterogeneous material (18). It has been demonstrated that improving bioactivity can be achieved by combining materials like carbonatite hydroxyapatite (cHA) and polylactic acid (PLA) to produce composite or hybrid scaffolds (6, 17, 19-20). Since the chemistry and structure of PLA/HA combine to more closely resemble genuine bone tissue than either ceramic or polymer material alone, this combination has drawn the attention of numerous researchers (21-24). In large mandibular bone defects, composite scaffolds consisting of PCL (polycaprolactone) mixed with a hydrogel infused with bioactive compounds (resveratrol and strontium ranelate) can significantly enhance bone regeneration (57). Additionally, there aren't many studies that show the effect assessment of the mandibular region; instead, the majority of these findings focus on the maxilla region. However, the mandible region is just as significant as the maxilla region as it is impossible to predict the direction of contact when playing sports (25-28).

Composite scaffolds composed of TCL (terephthaloyl chloride) blended with magnesium can also indorse bone healing (15, 57).

Additionally, numerable of studies have established the osteogenic potential of nano-hydroxyapatite in combination with composite polymeric scaffolds (29-30). Scaffolds made of metal have also produced excellent outcomes. Titanium, as a metallic biomaterial, is beneficial for biomedical applications because of its sustainability in additive manufacturing, which reduces material waste and environmental impact (31). Porous titanium scaffolds have demonstrated good results in extensive bone defects in multiple clinical studies (9, 32). Titanium and its alloys are widely consumed in dental and orthopaedic applications for their outstanding corrosion resistance, formability, and fatigue strength, with Plasma Electrolytic Oxidation (PEO) surface modifications further enhancing implant-cell connections for optimal long-term clinical performance. (33) Advances in biomaterials and 3D printing have enabled the creation of customized bone scaffolds with complex properties and shapes, focusing on the design, optimization, and manufacturing processes to improve bone tissue repair. (34) 3D printing, a form of additive manufacturing, has gained popularity quickly for uses in bone restoration. Indeed, a commercially/clinically available, FDA-approved 3D-printed scaffold for bone regeneration is accessible for spinal fusions (35, 57). The ability to customize the scaffold's mechanics, pace of deterioration, and biological impact through a vast array of geometries, pore sizes, and materials is one of the core benefits of employing 3D printing for scaffolds (36). Studies show understanding material properties is crucial for scaffold design and optimization. The choice of using traditional materials (e.g. carbon steel, etc.) or newer materials (e.g. epoxy resin, carbon fibre, etc.) should be made after thorough research (37). Research into infill patterns for additive manufacturing reveals that triangular patterns generally exhibit lower stress levels compared to rectangular patterns, suggesting that optimization of infill can enhance scaffold performance (38).

Numerous polymeric materials have high rigidities and are bioresorbable, which means that new tissue will gradually replace them after implantation and support from bone regeneration (27, 39). For instance, PLA is a material that is frequently used to replace bone tissue due to its exceptional biocompatibility and biodegradability (1-2, 40-41) as well as its strong mechanical qualities (40-41). Its efficacy in replacing trabecular bone has been demonstrated (2, 40).

It is also a widely accessible and reasonably priced material. We have demonstrated that inexpensive 3D printers can produce scaffolds with different pore sizes to regulate stem cell differentiation (1, 36, 42-44, 57). Additionally, we have demonstrated that beta-tricalcium phosphate or hydroxyapatite-containing composite scaffolds can also initiate stem cell differentiation and encourage bone repair in animal models (45-48, 57). Titanium (Ti) and its alloy Ti-6Al-4V are used in 3D printing for orthopaedic implants due to their ability to create complex, patientspecific designs with precise mechanical characteristics and porous structures (49). These findings are consistent with the findings of other groups. The three most important characteristics for scaffold design are porosity, pore size, and pore configuration. Osteogenesis is encouraged by porosity because it enhances surface area and permits cell movement (9). Infill density and patterns, such as line and triangle, have shown significant effects on tensile and bending strengths, indicating the importance of precise structural design in 3D-printed scaffolds (50).

For instance, vascularization is encouraged by porosities greater than 50% (51). A trade-off between porosity, strength, and osseointegration appears to be necessary, as excessive porosity is unlikely to meet the high mechanical strength needed for bone use (9). In fact, scaffold rigidity does indeed decrease linearly with increasing scaffold porosity (21). Scaffolds must be constructed to favor the type of cells and tissues they want to replace, as previous research has demonstrated that pore size and density affect cellular development and adhesion (17, 52-53). Keeping in mind that sufficient cell proliferation and osteogenesis are required, we set out to investigate different combinations of pore geometry, pore size, and pore arrangement in order to identify the combination offering the best mechanical qualities (57). Additionally, we assessed the effects of two printing orientations (fibre alignment) on the stiffness of the scaffold. parameter and discovered that the filaments can withstand the mechanical load more effectively when they are associated with the direction of the compressive loading than when they are perpendicular (54-56, 57).

3. Material and Methods

3.1. Test Materials: (i) PLA (ii) SS316L

The study involves analyzing test samples collected of Stainless Steel (316) and PLA material, commonly utilized in 3D Printing, to assess their compressive strength. PLA is suitable for artistic models, educational projects, and prototyping, it is less suitable for high-impact or high-temperature applications. Due to its excellent surface finish and wide range of colour, PLA is the most frequently utilized material in 3D printing. Stainless steel (316L) is suitable because of its exceptional strength and resistance to corrosion, stainless steel 316L finds application in the food and beverage sector, medical devices, and maritime environments. It is also extensively utilized in building, pharmaceuticals, and chemical processing. It is perfect for various industrial and commercial applications because of its durability and bio-compatibility.

3.2. Software linked with Printer

The CAD software generates an initial 3D model, which is then saved with STL file extension. Next, the STL file is imported into Ultimaker Cura 5.1.1, a program that slices the 3D object horizontally (ref Fig. 1).

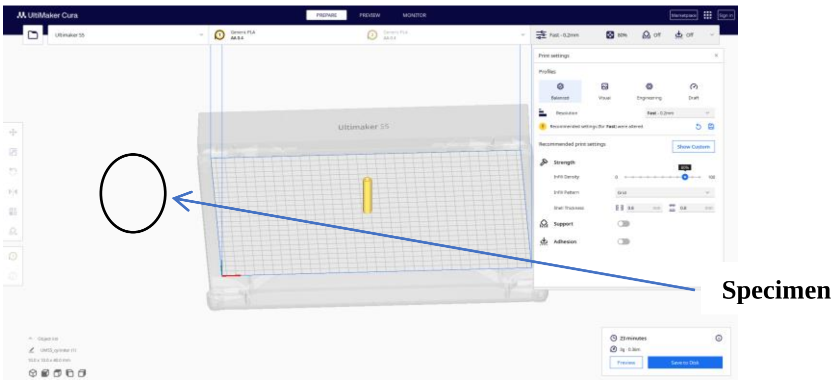

Fig. 1: Sliced specimen

Various printing parameters such as layer height, layer speed, layer thickness, print speed, infill rate, printing temperatures, support structure, print orientation, and other factors are configured within the slicing software. To achieve higher melting temperatures for the prints, a glass sheet substrate is intentionally utilized, while confirming that the platform temperature aligns with the supplier's recommendations. Segments of the G-code file are then sent to the FDM machine for printing. The extruder heats the nozzle and built-in platform prior to extruding the material. A polymeric filament is squeezed out from the heated nozzle head onto the building platform. Fig. 2 illustrates an FDM machine, while Fig. 3 shows that 3D printer. In addition to other requirements, the produced parts need to withstand repeated loads and significant temperature changes. However, due to issues such as warping and contraction during printing, detachment from the platform, and gas emissions, it may not be suitable for many applications. The specimen attributes in Table 1 & 2 are provided by the manufacturer for use in this project.

4. Printing Process and Parameters

4.1 Printing Process

The dimension of the solid polymer compression sample is 20 mm lengthwise and of a diameter of 6 mm. For the hollow sample, the dimensions are the external diameter as 10 mm, the internal diameter as 6 mm, and the total length is 20 mm. Stainless steel sample dimensions are 6 mm diameter and 20 mm length.

The compression test specimens are produced in an AM facility with 80% infill density using an Ultimaker 2 + FDM machine. To produce the compression specimens, grid pattern is used.

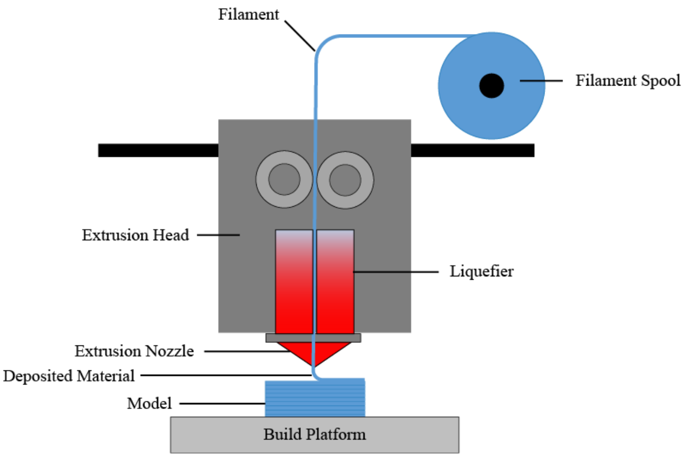

Fig. 2: Illustrative FDM machine

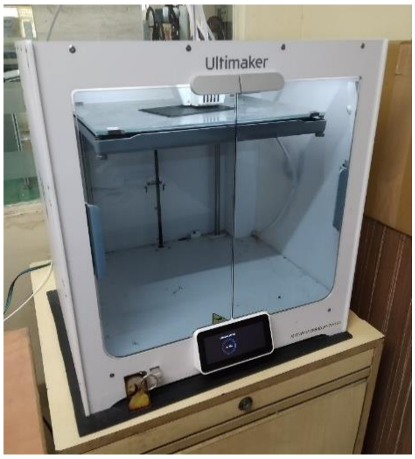

Fig. 3: 3D Printer

4.2 Material Properties

Table 1: Properties of PLA Material

Mechanical Properties	Values
Density	1.43 g/cm^3
Young's Modulus	4.5 GPa
Melting temp.	150-180°C
Biodegradability	Biodegradable under industrial composting condition
Poisson's Ratio	0.34

Table 2: Properties of Stainless steel (316) Material

Mechanical Properties	Values

Density	8 g/cm^3
Young's Modulus	193 GPa
Melting temp.	1375-1400 ℃
Biodegradability	Biodegradable under industrial composting condition
Poisson's Ratio	0.3

4.3 Printing process parameters

Printing process parameters are tabulated in Table 3.

Table 3: Printing process parameters

Nozzle diameter	Layer height	0.4 mm
Layer height		**0.2 mm**
	First layer height	0.8 mm
Shells	Perimeter shells	0
	Top solid layers	0
	Bottom solid layers	0
Infill	Fill density	80% (compression hollow) 80%(compression solid)
	Fill Pattern	Grid
Speed	Print speed	45 mm/s
	Travel speed	120 mm/s
Temperature	Left extruder	230 ℃
	Platform	105 ℃
Type of printing	Fine	
Printing time	Sample	23 minutes

5. Discussions based on Tests Conducted

5.1 Compression testing

Specimen Preparation

The two manufactured specimens of PLA – hollow and 80% infill solid and the Stainless Steel 316L specimen are as shown in the Fig. 4, 5 & 6 below.

Fig. 4: PLA specimen (Hollow)

Fig. 5: PLA specimen (80% (Solid)

Fig. 6: SS 316L specimen

5.2 Test Protocols

These specimens are tested on Universal Testing Machine for determining their compressive strength. Fig.7, shows that Schematic diagram of compression testing setup.

The following procedure is followed:

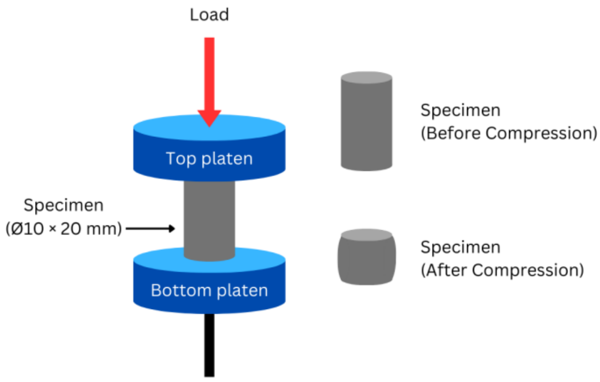

Fig. 7: Schematic Diagram of Compression Testing

During the compression test, the material was measured while being compressed heavily. This test was carried out to determine the 3D-printed samples' compression strength. Compression strength is measured using the FSA M100 UTM tester, as illustrated in Fig.7, 8, 9.

The test was conducted at MIT World Peace University, Pune using a 10-kN weight cell moving at a constant speed of 1 mm per minute. After inserting the samples through the handles of the UTM, the force was progressively increased until the samples failed. The material's compression strength is determined using the resulting buckle. Fig.10, 11 shows the samples after compression test.

5.3 Test Outcome and Result

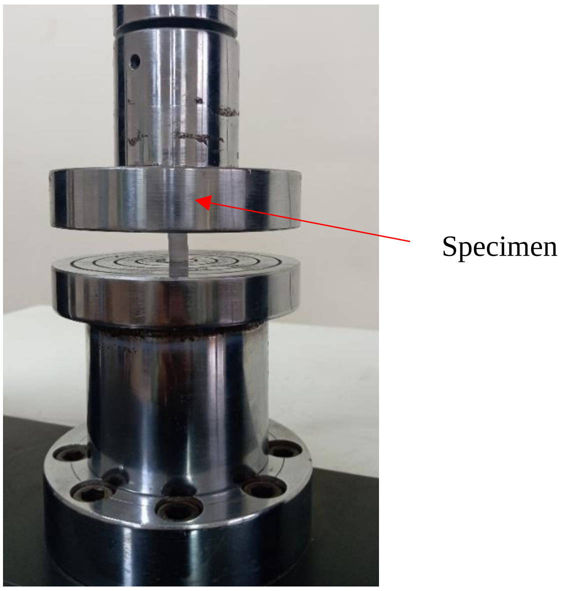

Fig. 8: Compression Testing of Polymer

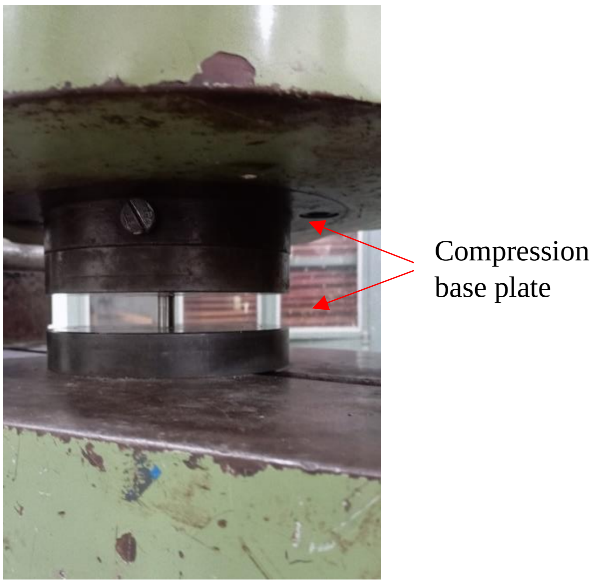

Fig. 9: Compression Testing of Steel

For solid PLA sample with 80% infill the Compressive strength was 29.770 N/mm2, and the test sample were subjected to axial load of 2066 N during the test.

For hollow PLA sample compressive strength was 34.189 N/mm2, and test sample were subjected to axial load of 1508 N during test.

For Solid stainless steel 316L sample compressive strength was 229 N/mm2, and test sample were subjected to axial load of 176580 N during test.

The ultimate compressive strength (σc) and maximum strain (εt) were estimated using equations 1 σc = F/A.

5.4 Analysis of Morphology of the tested samples

Fig. 10: Compressed Polymer Specimen

Fig. 11: Compressed Steel Specimen

SEM was used to examine the rupture that happened. All specimens were coated in platinum using Auto Fine Coater prior to the test, and to make sure the platinum had reached all intended surfaces. They were placed in the sputter coater for sixty seconds. The scanning was performed at MIT World Peace University, which was done using the TESCAN Scanning electron microscope (SEM) (refer Fig.12). The device employed a concentrated electron beam to scan a surface in order to produce a picture. Together, the samples and the electrons in the beam produced signals that allowed further analysis of the morphology for every percentage of PLA polymer. For the purpose of examining and testing the samples, three different magnifications were used: compression test 100 µm, 200 µm and 500 µm. Samples were placed on the specimen support and concentrated on the broken edge in order to discover voids, Cracks and porosity (refer Fig.12 (a), (b), (c) & (d)).

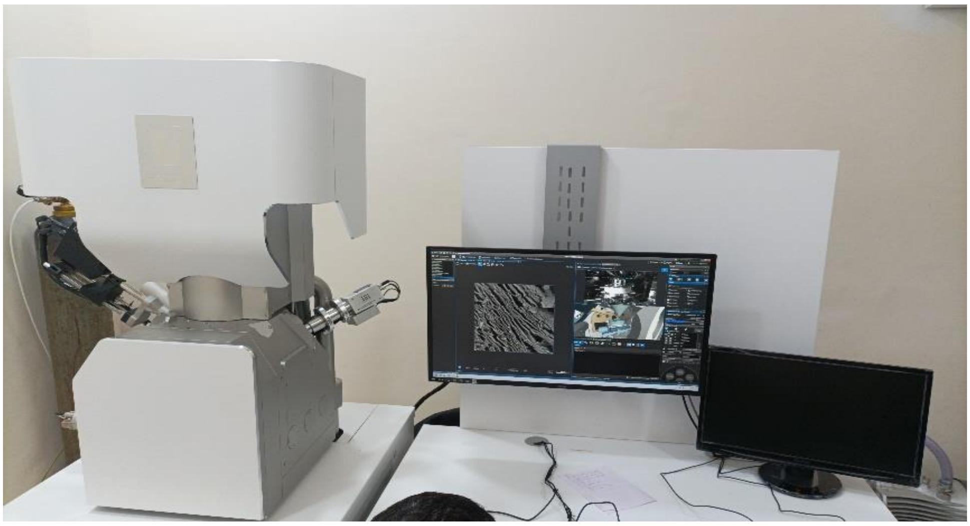

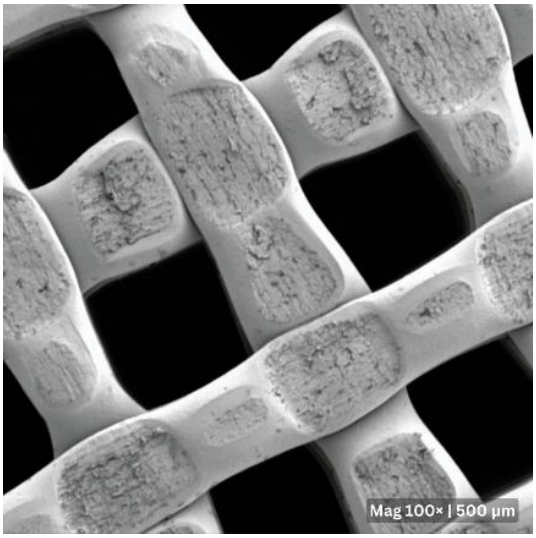

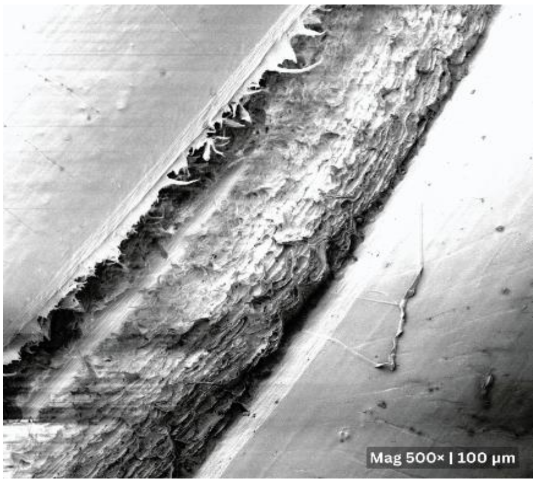

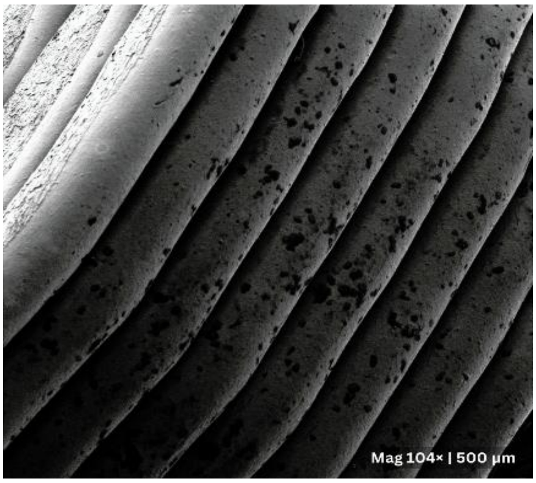

Fig.12 (c) Mag 500× | 100 µm

Fig.12 (d) Mag 104× | 500 µm

Fig. 12: SEM Setup

5.5 Analytical calculations

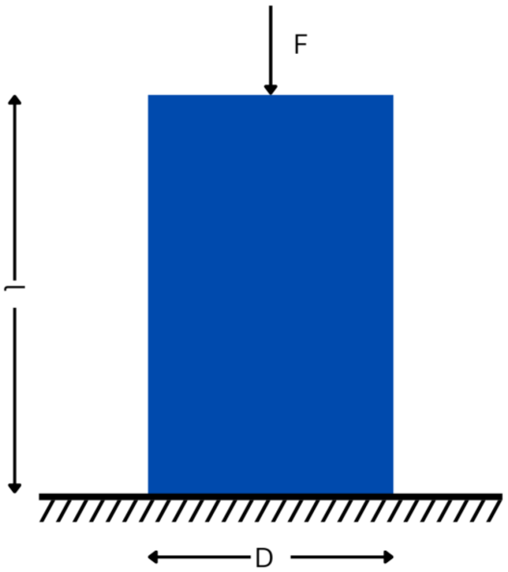

PLA & Steel (Solid Case 1 & 3)

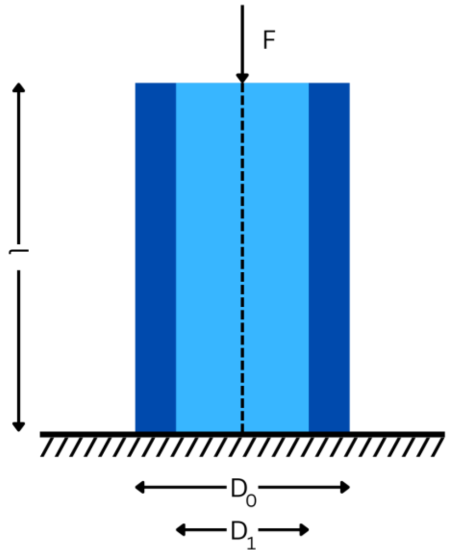

PLA (hollow Case 2)

Where,

L = Length of Specimen,

D = Diameter of specimen,

Di = Inner Diameter of specimen,

Do = Outer diameter of specimen,

F = Force,

A = Area of specimen

(A) For PLA 80% Infill Solid Specimen,

$A_s = \frac{\pi}{4} \times D^2 = 78.5\ mm^2$, Failure Load = 2066 N and compression strength = 29.770 N/mm^2

$\sigma = \frac{F}{A}$

$\sigma_1 = \frac{F1}{A} = 13.15$ MPa ;….. for 50% load

$\sigma_2 = \frac{F2}{A} = 21.05$ MPa ; ….. for 80% load

$\sigma_3 = \frac{F3}{A} = 26.318$ MPa……..failure load

Tuijin Jishu/Journal of Propulsion Technology
ISSN: 1001-4055
Vol. 45 No. 4 (2024)

(B) For PLA Hollow Specimen,

$A_s = \frac{\pi}{4} \times (D_0^2 - D_1^2) = 50.26\ mm^2$, Failure Load = 1508 N and compression strength = 34.180 MPa

$\sigma = \frac{F}{A}$

$\sigma_1 = \frac{F1}{A} = 15$ MPa ; ….. for 50% load

$\sigma_2 = \frac{F2}{A} = 24$ MPa ; ….. for 80% load

$\sigma_3 = \frac{F3}{A} = 30$ MPa……..failure load

(c) For Solid Steel Specimen,

$A_s = \frac{\pi}{4} \times D^2 = 78.5\ mm^2$, Failure Load = 176580 N and compression strength = 2248.567N/mm^2

$\sigma = \frac{F}{A}$

$\sigma_1 = \frac{F1}{A} = 1124.283$ MPa ; ….. for 50% load

$\sigma_2 = \frac{F2}{A} = 1798.853$ MPa ; ….. for 80% load

$\sigma_3 = \frac{F3}{A} = 2248.567$ MPa……..failure load

The analytical results are mentioned in Table 4 and plotted as shown in Fig. 13 (a), (b), & (c).

Table 4: Results of Analytical Calculations

	Parameters	Load	Solid Cylindrical Specimen	Load	Hollow Cylindrical Specimen	Load	Solid Steel
50% of failure load	Stress 1	1033	13.15	754	15	88290	1124.71
80% of failure load	Stress 2	1652.8	21.05	1206.4	24	141264	1799.54
100% of failure load	Stress 3	2066	26. 318	1508	30	176580	2249.42
	CS Area (mm$^{2)}$		29.77		34.18		

	Failure load		2066		1508		
	Elongation		3.66		3.94		
	Area		78.5		50.26		
	LENGTH		20		20		

(a)

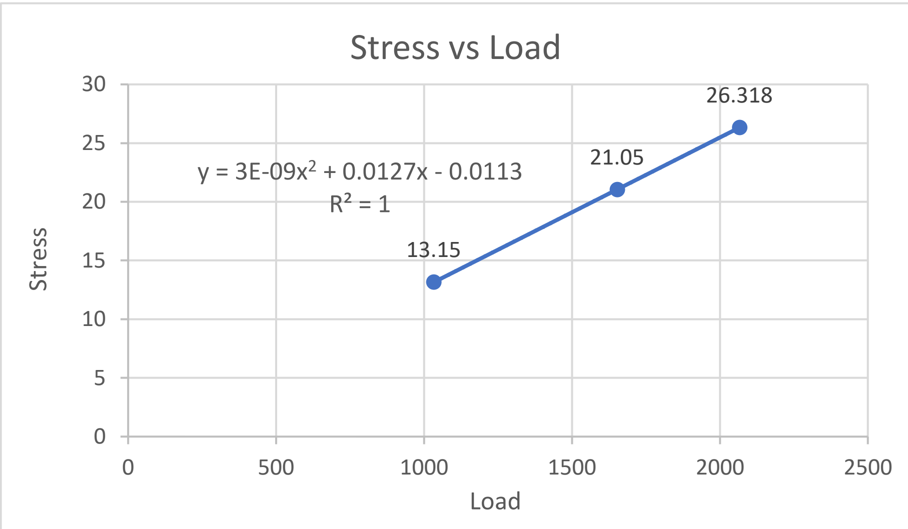

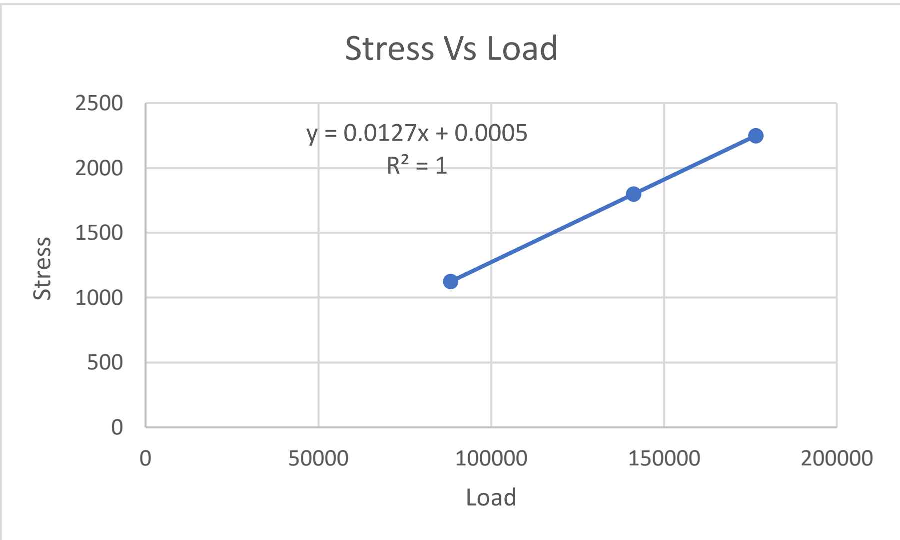

5.6 Calculations- Simulation

(b)

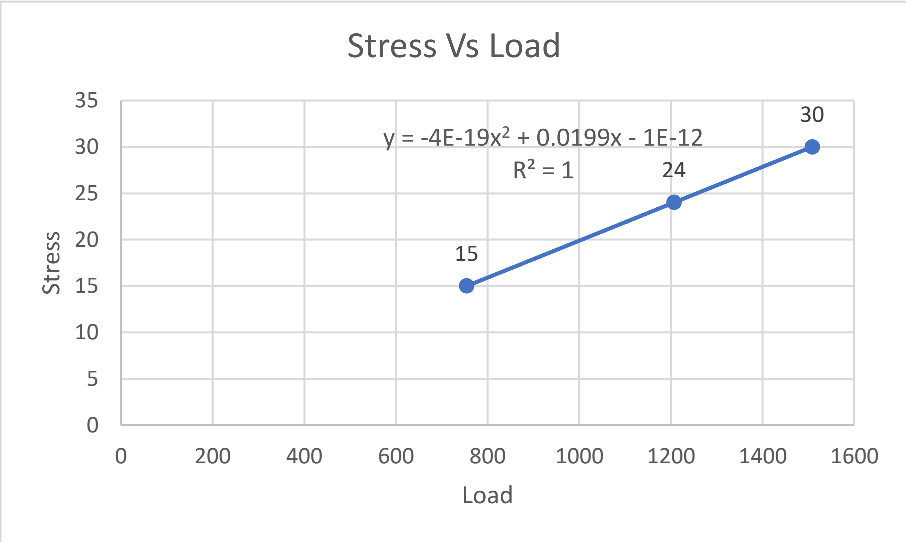

With simulations, following are the values of Von-Mises stress for materials considered:

Solid PLA- 28.124 MPa; Stainless Steel- 2252.789 MPa; Hollow PLA- 33.139 MPa

For Solid PLA= $\Delta_S = 1 - \left(\frac{\sigma m - \sigma s}{\sigma m}\right)$

$= 1 - (\frac{2252.789 - 28.124}{2252.789})$

$= 1 - 0.98751$

$= 0.01249$

$\therefore \boldsymbol{\sigma}_s = \Delta_S \, . \, \boldsymbol{\sigma}^m$

$= 0.01249 \, \boldsymbol{\sigma} m$

For Hollow PLA $\Delta_H = 1 - \left(\frac{\sigma m - \sigma H}{\sigma m}\right)$

$= 1 - (\frac{2252.789 - 33.139}{2252.789})$

$= 1 - 0.98528$

$= 0.01472$

$\therefore \boldsymbol{\sigma}_H = \Delta_H \, . \, \boldsymbol{\sigma}^m$

$= 0.01472 \, \boldsymbol{\sigma} m$

Calculations- Experimental

For Solid PLA $\Delta_S = 1 - \left(\frac{\sigma 2 - \sigma 1}{\sigma 1}\right)$

$= 1 - \left(\frac{\sigma m - \sigma s}{\sigma m}\right)$

$= 1 - (\frac{2248 - 26}{2248})$

$= 0.01157$

$\therefore \boldsymbol{\sigma}_s = \Delta_S \, . \, \boldsymbol{\sigma}^m$

$= 0.01157 \, \boldsymbol{\sigma} m$

Where,

$\boldsymbol{\sigma}_m$ is maximum stress induced in SS316L

$\boldsymbol{\sigma}_s$ is maximum stress in 80% infill PLA

For Hollow PLA $\Delta_H = 1 - \left(\frac{\sigma m - \sigma s}{\sigma m}\right)$

$= 1 - (\frac{2248 - 30}{2248})$

$= 0.01335$

$\therefore \boldsymbol{\sigma}_H = \Delta_S \, . \, \boldsymbol{\sigma}^m$

$= 0.01335 \, \boldsymbol{\sigma}_m$

Where,

$\boldsymbol{\sigma}_m$ is maximum stress induced in SS316L

$\boldsymbol{\sigma}_H$ is maximum stress in hollow PLA

5.7 FE Simulation

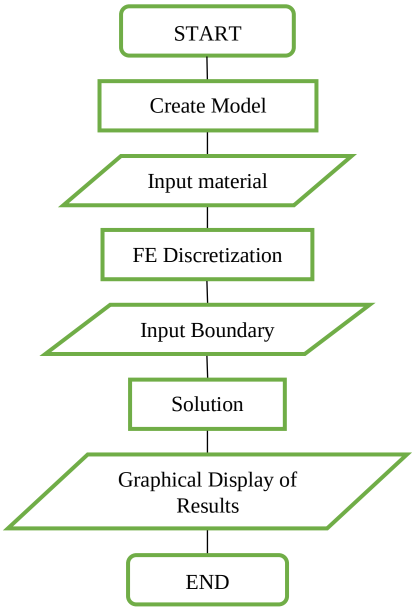

(a)

(b)

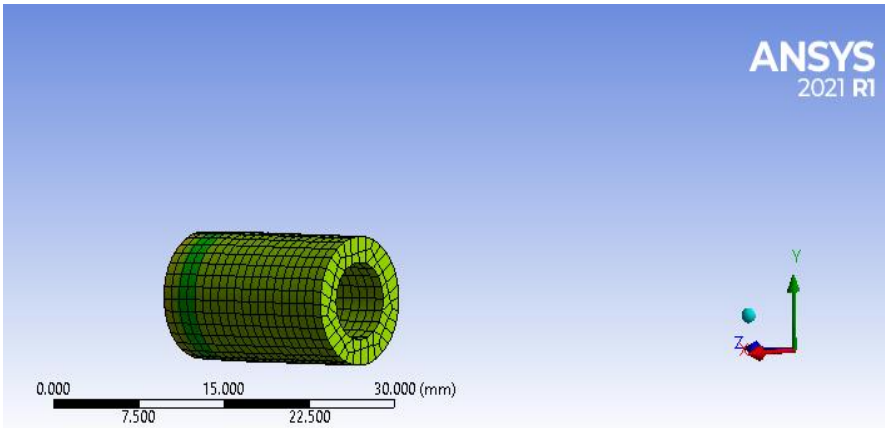

(c)

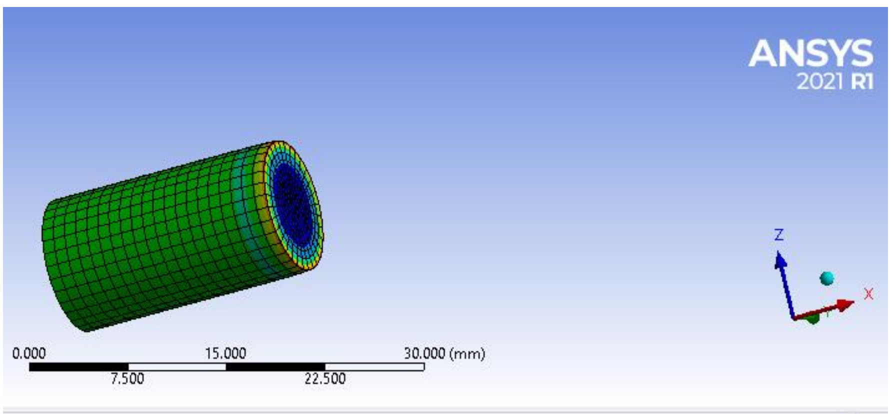

(d)

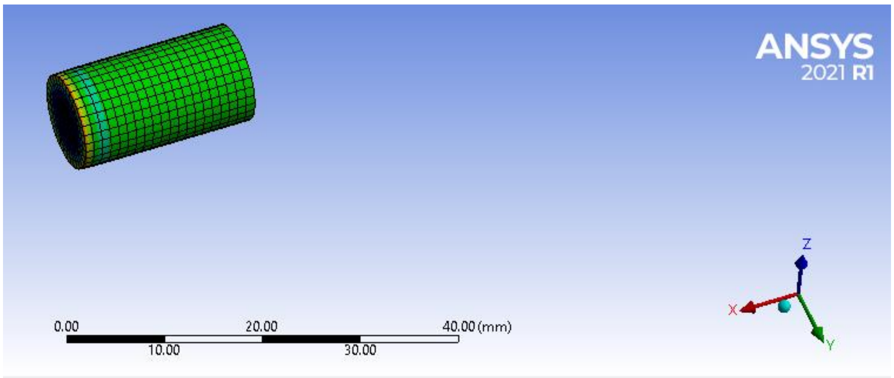

Fig. 14 (a) FEA Flowchart for Hollow PLA , (b) FEA Results of Von-Mises stress for Hollow PLA (c) FEA Results of Von-mises stress for PLA (d) FEA Results of Von-mises stress for SS316L

5.8 Hollow PLA Cylinder

Figure 14 (a) explains the process of the simulation for a hollow PLA cylinder using Ansys Workbench. A 3D model was created in Catia V5, as shown in Fig. 14 (b). For material properties, PLA Polymer material was used (density = 1430 kg/m^3, Young's modulus = 4.5 GPa, and Poisson's ratio = 0.34). In FE discretization, meshing was performed, resulting in 6426 nodes and 1160 elements. All nodes on the bottom face were constrained for displacement, and a load of 1508 N was applied on the top face. A static analysis was conducted under maximum load conditions, yielding an equivalent stress of 33.139 MPa and a total deformation of 0.144 mm.

5.9 Solid PLA Cylinder

In the simulation (ref Fig 14 (c)), for material properties, PLA Polymer material was used (density = 1430 kg/m^3, Young's modulus = 4.5 GPa, and Poisson's ratio = 0.34). In FE discretization, meshing was performed, resulting in 19958 nodes and 4620 elements. All nodes on the bottom face were constrained for displacement, and a load of 2066 N was applied on the top face. A static analysis was conducted under maximum load conditions, yielding an equivalent stress of 28.124 MPa and a total deformation of 0.122 mm.

5.10 Solid SS316L (Stainless Steel)

In the simulation (ref Fig 14 (d)), for material properties, Solid SS316L (Stainless Steel) material was used (density = 8000 kg/m^3, Young's modulus = 193 GPa, and Poisson's ratio = 0.3). In FE discretization, meshing was performed, resulting in 20988 nodes and 4824 elements. All nodes on the bottom face were constrained for displacement, and a load of 176580 N was applied on the top face. A static analysis was conducted under maximum load conditions, yielding an equivalent stress of 2252.789 MPa and a total deformation of 0.222 mm.

6. Conclusions

With reference to the results and discussions, the following conclusions are drawn:

1) Three types of sample were tested in UTM solid SS316L, solid infill 80% PLA and hollow PLA considering possibility of introducing these as implantable material as substitute to bone.
2) Has be observed for the highest compressive strength (2248.567 N/mm2), followed by hollow polymer PLA specimen (34.29 N/mm2). Solid PLA specimen with 80% infill was found to be the weakest in compression (29.77 N/mm2)

3) Stainless Steel specimen SS316L exhibited the highest load carrying capacity till failure (1,76,580 N), followed by solid polymer PLA specimen with 80% infill (2066 N). The hollow PLA specimen could carry the lowest load (1508 N)
4) A static structural FEA simulation was performed. Solid PLA, Hollow PLA and Solid SS316L specimen showed von-Mises stresses of 28.124 N/mm2, 33.139 N/mm2 and 2252.789 N/mm2 respectively. These FEA results were found to be within 10% range of the experimental ones, thus achieving validation.
5) The strength-to-weight ratio of stainless steel specimen seen to be highest (120.372), followed by hollow PLA specimen (32.657). The Solid PLA specimen with 80% infill showed the lowest strength-to-weight ratio (22.725)
6) The cost incurred for 3D printing PLA materials is considerably less than that for Stainless Steel SS316L.
7) In all, considering the high compressive strength, medium strength-to-weight ratio, reasonable load carrying capacity, biocompatibility, high accuracy and comparatively low cost of manufacturing using 3D printing, hollow PLA material is the choice seen as a substitute for bone and bone interface in biomedical applications.

List of Abbreviations

FDM- Fused Deposition Modelling

SLA- Stereolithography

SLS- Selective Laser Sintering

FFF- Fused Filament Fabrication

AM- Additive Manufacturing

3D- Three Dimensional

ABS- Acrylonitrile Butadiene Styrene

SEM- Scanning Electron Microscopy

CAD- Computer-aided Design

STL- Stereolithography

PLA- Polylactic Acid

mm- millimetre

°C- degree Celsius

hr- hour

min- minutes

UTM- Universal Testing Machine

kN- kilo Newton

N/mm2- Newton per square meter

N- Newton

Vs- Versus

mm2- square millimetre

MIT WPU- MIT World Peace University

mm/min- millimetre per minute

nm- Newton-meter

µm- micrometre

MPa- Mega Pascal

$\boldsymbol{\sigma}$m is maximum stress induced in SS316L

$\boldsymbol{\sigma}$s is maximum stress in 80% infill PLA

Declarations

Availability of data and materials: The data supporting the findings of this study are provided in the article and can be obtained from the corresponding author upon request.

Competing interests: No conflict of interest has been declared by the authors.

Funding: NA

Authors' Contributions:

"AS hypothesized the study and conducted the experiments. RG handled data compilation and editing. PS deduced and visualized the data. SB managed the administration of the project. The document has been studied and consented by all the authors."

Acknowledgements: NA

Refrences

[1] Fairag, R., Rosenzweig, D. H., Ramirez-Garcialuna, J. L., Weber, M. H., & Haglund, L. (2019). Three-Dimensional printed polylactic acid scaffolds promote bone-like matrix deposition in vitro. ACS Applied Materials & Interfaces, 11(17), 15306–15315. https://doi.org/10.1021/acsami.9b02502

[2] Baptista, R., & Guedes, M. (2021). Morphological and mechanical characterization of 3D printed PLA scaffolds with controlled porosity for trabecular bone tissue replacement. Materials Science and Engineering C, 118, 111528. https://doi.org/10.1016/j.msec.2020.111528

[3] Roseti, L., Parisi, V., Petretta, M., Cavallo, C., Desando, G., Bartolotti, I., & Grigolo, B. (2017). Scaffolds for Bone Tissue Engineering: State of the art and new perspectives. Materials Science and Engineering C, 78, 1246–1262. https://doi.org/10.1016/j.msec.2017.05.017

[4] O'Keefe, R. J., & Mao, J. (2011). Bone Tissue Engineering and Regeneration: From Discovery to the Clinic—An Overview. Tissue Engineering Part B Reviews, 17(6), 389–392. https://doi.org/10.1089/ten.teb.2011.0475

[5] Pitaru, A. A., Lacombe, J., Cooke, M. E., Beckman, L., Steffen, T., Weber, M. H., Martineau, P. A., & Rosenzweig, D. H. (2020). Investigating Commercial Filaments for 3D Printing of Stiff and Elastic Constructs with Ligament-Like Mechanics. Micromachines, 11(9), 846. https://doi.org/10.3390/mi11090846

[6] Oladapo, B. I., Zahedi, S., & Adeoye, A. (2019). 3D printing of bone scaffolds with hybrid biomaterials. Composites Part B Engineering, 158, 428–436. https://doi.org/10.1016/j.compositesb.2018.09.065Yan, Y., Chen, H., Zhang, H., Guo, C., Yang, K., Chen, K., Cheng, R., Qian, N., Sandler, N., Zhang, Y. S., Shen, H., Qi, J., Cui, W., & Deng, L. (2019). Vascularized 3D printed scaffolds for promoting bone regeneration. Biomaterials, 190–191, 97–110. https://doi.org/10.1016/j.biomaterials.2018.10.033

[7] Su, X., Wang, T., & Guo, S. (2021). Applications of 3D printed bone tissue engineering scaffolds in the stem cell field. Regenerative Therapy, 16, 63–72. https://doi.org/10.1016/j.reth.2021.01.007

[8] Zhang, L., Yang, G., Johnson, B. N., & Jia, X. (2019). Three-dimensional (3D) printed scaffold and material selection for bone repair. Acta Biomaterialia, 84, 16–33. https://doi.org/10.1016/j.actbio.2018.11.039

[9] Aravamudhan, A., Ramos, D. M., Nip, J., Subramanian, A., James, R., Harmon, M. D., Yu, X., & Kumbar, S. G. (2013). Osteoinductive small molecules: growth factor alternatives for bone tissue engineering. Current Pharmaceutical Design, 19(19), 3420–3428. https://doi.org/10.2174/1381612811319190008

[10] Cheng, C., Shie, M., Lai, Y., Foo, N., Lee, M., & Yao, C. (2021). Fabrication of 3D Printed Poly(lactic acid)/Polycaprolactone Scaffolds Using TGF-β1 for Promoting Bone Regeneration. Polymers, 13(21), 3731. https://doi.org/10.3390/polym13213731

[11] Cubo-Mateo, N., & Rodríguez-Lorenzo, L. M. (2020). Design of Thermoplastic 3D-Printed scaffolds for bone tissue engineering: Influence of parameters of "Hidden" importance in the physical properties of scaffolds. Polymers, 12(7), 1546. https://doi.org/10.3390/polym12071546

[12] Nyberg, E., Holmes, C., Witham, T., & Grayson, W. L. (2015). Growth factor-eluting technologies for bone tissue engineering. Drug Delivery and Translational Research, 6(2), 184–194. https://doi.org/10.1007/s13346-015-0233-3

[13] Murphy, S. V., & Atala, A. (2014). 3D bioprinting of tissues and organs. Nature Biotechnology, 32(8), 773–785. https://doi.org/10.1038/nbt.2958

[14] Dong, Q., Zhang, M., Zhou, X., Shao, Y., Li, J., Wang, L., Chu, C., Xue, F., Yao, Q., & Bai, J. (2021). 3D-printed Mg-incorporated PCL-based scaffolds: A promising approach for bone healing. Materials Science and Engineering C, 129, 112372. https://doi.org/10.1016/j.msec.2021.112372

[15] Ahangar, P., Aziz, M., Rosenzweig, D. H., & Weber, M. H. (2019). Advances in personalized treatment of metastatic spine disease. Annals of Translational Medicine, 7(10), 223. https://doi.org/10.21037/atm.2019.04.41

[16] Turnbull, G., Clarke, J., Picard, F., Riches, P., Jia, L., Han, F., Li, B., & Shu, W. (2018). 3D bioactive composite scaffolds for bone tissue engineering. Bioactive Materials, 3(3), 278–314. https://doi.org/10.1016/j.bioactmat.2017.10.001

[17] Boskey, A. L., & Roy, R. (2008). Cell culture systems for studies of bone and tooth mineralization. Chemical Reviews, 108(11), 4716–4733. https://doi.org/10.1021/cr0782473

[18] Buyuksungur, S., Tanir, T. E., Buyuksungur, A., Bektas, E. I., Kose, G. T., Yucel, D., Beyzadeoglu, T., Cetinkaya, E., Yenigun, C., Tönük, E., Hasirci, V., & Hasirci, N. (2017). 3D printed poly(ε-caprolactone) scaffolds modified with hydroxyapatite and poly(propylene fumarate) and their effects on the healing of rabbit femur defects. Biomaterials Science, 5(10), 2144–2158. https://doi.org/10.1039/c7bm00514h

[19] Trachtenberg, J. E., Placone, J. K., Smith, B. T., Fisher, J. P., & Mikos, A. G. (2017). Extrusion-based 3D printing of poly(propylene fumarate) scaffolds with hydroxyapatite gradients. Journal of Biomaterials Science Polymer Edition, 28(6), 532–554. https://doi.org/10.1080/09205063.2017.1286184

[20] Zhang, B., Wang, L., Song, P., Pei, X., Sun, H., Wu, L., Zhou, C., Wang, K., Fan, Y., & Zhang, X. (2021). 3D printed bone tissue regenerative PLA/HA scaffolds with comprehensive performance optimizations. Materials & Design, 201, 109490. https://doi.org/10.1016/j.matdes.2021.109490

[21] Gong, B., Cui, S., Zhao, Y., Sun, Y., & Ding, Q. (2017). Strain-controlled fatigue behaviors of porous PLA-based scaffolds by 3D-printing technology. Journal of Biomaterials Science Polymer Edition, 28(18), 2196–2204. https://doi.org/10.1080/09205063.2017.1388993

[22] Rosenzweig, D., Carelli, E., Steffen, T., Jarzem, P., & Haglund, L. (2015). 3D-Printed ABS and PLA scaffolds for cartilage and nucleus pulposus tissue regeneration. International Journal of Molecular Sciences, 16(7), 15118–15135. https://doi.org/10.3390/ijms160715118

[23] Shuhua, W., Qiaoli, X., Fen, L., Jinming, D., Husheng, J., & Bingshe, X. (2013). Preparation and properties of cellulose-based carbon microsphere/poly(lactic acid) composites. Journal of Composite Materials, 48(11), 1297–1302. https://doi.org/10.1177/0021998313485263

[24] Zhang, W., Shi, W., Wu, S., Kuss, M., Jiang, X., Untrauer, J. B., Reid, S. P., & Duan, B. (2020). 3D printed composite scaffolds with dual small molecule delivery for mandibular bone regeneration. Biofabrication, 12(3), 035020. https://doi.org/10.1088/1758-5090/ab906e

[25] Ratnakar R. Ghorpade, Kiran Bagal, Ketan Karandikar, Contemporary studies on suitability of biomaterials for mouth-guards, Materials Today: Proceedings, Volume 47, Part 16, 2021, Pages 5601-5606, ISSN 2214-7853, https://doi.org/10.1016/j.matpr.2021.03.605

[26] Jeong, H., Gwak, S., Seo, K. D., Lee, S., Yun, J., Cho, Y., & Lee, S. (2020). Fabrication of Three-Dimensional composite scaffold for simultaneous alveolar bone regeneration in dental implant installation. International Journal of Molecular Sciences, 21(5), 1863. https://doi.org/10.3390/ijms21051863

[27] Olubamiji, A. D., Izadifar, Z., Si, J. L., Cooper, D. M. L., Eames, B. F., & Chen, D. X. (2016). Modulating mechanical behaviour of 3D-printed cartilage-mimetic PCL scaffolds: influence of molecular weight and pore geometry. Biofabrication, 8(2), 025020. https://doi.org/10.1088/1758-5090/8/2/025020

[28] Bordea, I. R., Candrea, S., Alexescu, G. T., Bran, S., Băciuț, M., Băciuț, G., Lucaciu, O., Dinu, C. M., & Todea, D. A. (2020). Nano-hydroxyapatite use in dentistry: a systematic review. Drug Metabolism Reviews, 52(2), 319–332. https://doi.org/10.1080/03602532.2020.1758713

[29] Ji, X., Yuan, X., Ma, L., Bi, B., Zhu, H., Lei, Z., Liu, W., Pu, H., Jiang, J., Jiang, X., Zhang, Y., & Xiao, J. (2020). Mesenchymal stem cell-loaded thermosensitive hydroxypropyl chitin hydrogel combined with a three-dimensional-printed poly(ε-caprolactone) /nano-hydroxyapatite scaffold to repair bone defects via osteogenesis, angiogenesis and immunomodulation. Theranostics, 10(2), 725–740. https://doi.org/10.7150/thno.39167

[30] Pesode, P., & Barve, S. (2023). Additive manufacturing of metallic biomaterials: sustainability aspect, opportunity, and challenges. Journal of Industrial and Production Engineering, 40(6), 464–505. https://doi.org/10.1080/21681015.2023.2229341

[31] Baptista, R., & Guedes, M. (2021). Porosity and pore design influence on fatigue behavior of 3D printed scaffolds for trabecular bone replacement. Journal of the Mechanical Behavior of Biomedical Materials/Journal of Mechanical Behavior of Biomedical Materials, 117, 104378. https://doi.org/10.1016/j.jmbbm.2021.104378

[32] Pesode, P., & Barve, S. (2021). Surface modification of titanium and titanium alloy by plasma electrolytic oxidation process for biomedical applications: A review. Materials Today Proceedings, 46, 594–602. https://doi.org/10.1016/j.matpr.2020.11.294

[33] Bahraminasab, M. (2020). Challenges on optimization of 3D-printed bone scaffolds. BioMedical Engineering OnLine, 19(1). https://doi.org/10.1186/s12938-020-00810-2

[34] Stryker's spine division receives FDA clearance for 3D-Printed Tritanium TL curved posterior lumbar cage. (n.d.). Stryker. https://www.stryker.com/us/en/about/news/2018/stryker_s-spine-division-receives-fda-clearance-for-3d-printed-t.html

[35] Haglund, L., Ahangar, P., & Rosenzweig, D. H. (2019). Advancements in 3D printed scaffolds to mimic matrix complexities for musculoskeletal repair. Current Opinion in Biomedical Engineering, 10, 142–148. https://doi.org/10.1016/j.cobme.2019.06.002

[36] Karad, A. S., Sonawwanay, P. D., & Bachhav, C. Y. (2023). Finite element analysis of coil spring by using carbon fibre, carbon steel and epoxy resin materials. Materials Today Proceedings. https://doi.org/10.1016/j.matpr.2023.02.261

[37] Karad, A. S., Sonawwanay, P. D., Naik, M., & Thakur, D. (2023). Experimental tensile strength analysis of ABS material through FDM technique. Materials Today Proceedings. https://doi.org/10.1016/j.matpr.2023.09.216

[38] Polo-Corrales, L., Latorre-Esteves, M., & Ramirez-Vick, J. E. (2014). Scaffold design for bone regeneration. Journal of Nanoscience and Nanotechnology, 14(1), 15–56. https://doi.org/10.1166/jnn.2014.9127

[39] Grémare, A., Guduric, V., Bareille, R., Heroguez, V., Latour, S., L'heureux, N., Fricain, J., Catros, S., & Nihouannen, D. L. (2017). Characterization of printed PLA scaffolds for bone tissue engineering. Journal of Biomedical Materials Research Part A, 106(4), 887–894. https://doi.org/10.1002/jbm.a.36289

[40] Gregor, A., Filová, E., Novák, M., Kronek, J., Chlup, H., Buzgo, M., Blahnová, V., Lukášová, V., Bartoš, M., Nečas, A., & Hošek, J. (2017). Designing of PLA scaffolds for bone tissue replacement fabricated by

ordinary commercial 3D printer. Journal of Biological Engineering, 11(1). https://doi.org/10.1186/s13036-017-0074-3

[41] Velioglu, Z. B., Pulat, D., Demirbakan, B., Ozcan, B., Bayrak, E., & Erisken, C. (2018). 3D-printed poly(lactic acid) scaffolds for trabecular bone repair and regeneration: scaffold and native bone characterization. Connective Tissue Research, 60(3), 274–282. https://doi.org/10.1080/03008207.2018.1499732

[42] Holzapfel, B. M., Rudert, M., & Hutmacher, D. W. (2017). Gerüstträgerbasiertes Knochen-Tissue-Engineering. Der Orthopäde, 46(8), 701–710. https://doi.org/10.1007/s00132-017-3444-0

[43] Ferlin, K. M., Prendergast, M. E., Miller, M. L., Kaplan, D. S., & Fisher, J. P. (2016). Influence of 3D printed porous architecture on mesenchymal stem cell enrichment and differentiation. Acta Biomaterialia, 32, 161–169. https://doi.org/10.1016/j.actbio.2016.01.007

[44] Leukers, B., Gülkan, H., Irsen, S. H., Milz, S., Tille, C., Schieker, M., & Seitz, H. (2005). Hydroxyapatite scaffolds for bone tissue engineering made by 3D printing. Journal of Materials Science Materials in Medicine, 16(12), 1121–1124. https://doi.org/10.1007/s10856-005-4716-5

[45] Yuan, J., Zhen, P., Zhao, H., Chen, K., Li, X., Gao, M., Zhou, J., & Ma, X. (2014). The preliminary performance study of the 3D printing of a tricalcium phosphate scaffold for the loading of sustained release anti-tuberculosis drugs. Journal of Materials Science, 50(5), 2138–2147. https://doi.org/10.1007/s10853-014-8776-0

[46] Corcione, C. E., Gervaso, F., Scalera, F., Padmanabhan, S. K., Madaghiele, M., Montagna, F., Sannino, A., Licciulli, A., & Maffezzoli, A. (2019). Highly loaded hydroxyapatite microsphere/ PLA porous scaffolds obtained by fused deposition modelling. Ceramics International, 45(2), 2803–2810. https://doi.org/10.1016/j.ceramint.2018.07.297

[47] Barati, D., Shariati, S. R. P., Moeinzadeh, S., Melero-Martin, J. M., Khademhosseini, A., & Jabbari, E. (2016). Spatiotemporal release of BMP-2 and VEGF enhances osteogenic and vasculogenic differentiation of human mesenchymal stem cells and endothelial colony-forming cells co-encapsulated in a patterned hydrogel. Journal of Controlled Release, 223, 126–136. https://doi.org/10.1016/j.jconrel.2015.12.031

[48] Pesode, P., & Barve, S. (2022). Additive manufacturing of metallic biomaterials and its biocompatibility. Materials Today Proceedings. https://doi.org/10.1016/j.matpr.2022.11.248

[49] Karad, A. S., Sonawwanay, P. D., Naik, M., & Thakur, D. G. (2023b). Experimental study of effect of infill density on tensile and flexural strength of 3D printed parts. Journal of Engineering and Applied Science, 70(1). https://doi.org/10.1186/s44147-023-00273-x

[50] Wang, M. O., Vorwald, C. E., Dreher, M. L., Mott, E. J., Cheng, M., Cinar, A., Mehdizadeh, H., Somo, S., Dean, D., Brey, E. M., & Fisher, J. P. (2014). Evaluating 3D-Printed biomaterials as scaffolds for vascularized bone tissue engineering. Advanced Materials, 27(1), 138–144. https://doi.org/10.1002/adma.201403943

[51] Zeltinger, J., Sherwood, J. K., Graham, D. A., Müeller, R., & Griffith, L. G. (2001). Effect of pore size and void fraction on cellular adhesion, proliferation, and matrix deposition. Tissue Engineering, 7(5), 557–572. https://doi.org/10.1089/107632701753213183

[52] O'Brien, F., Harley, B., Yannas, I., & Gibson, L. (2005). The effect of pore size on cell adhesion in collagen-GAG scaffolds. Biomaterials, 26(4), 433–441. https://doi.org/10.1016/j.biomaterials.2004.02.052

[53] Zhang, B., Guo, L., Chen, H., Ventikos, Y., Narayan, R. J., & Huang, J. (2020). Finite element evaluations of the mechanical properties of polycaprolactone/hydroxyapatite scaffolds by direct ink writing: Effects of pore geometry. Journal of the Mechanical Behavior of Biomedical Materials/Journal of Mechanical Behavior of Biomedical Materials, 104, 103665. https://doi.org/10.1016/j.jmbbm.2020.103665

[54] Chetan Mohanlal Wani , Sachin Ratnakar Deshmukh, Ratnakar Raghunath Ghorpade, Studies on Stress Analysis of Hip Prosthesis Implant, Journal of Engineering Research and Sciences, 1(8): 01-11, 2022, Received: 28 February, 2022, Accepted: 20 July, 2022, Online: 19 August, 2022 DOI: https://dx.doi.org/10.55708/js0108001

[55] Vasuudhaa Sonawane, Ratnakar Ghorpade 'Overview of Mechanics of Porous Dental Implants', Techno-Societal 2022, Springer, page 577-585 (https://www.springerprofessional.de/overview-of-mechanics-of-porous-dental-implants/26078290)

[56] Chetan Patil, Ratnakar R. Ghorpade, Rajesh Askhedkar, Impact of structural parameterson the acoustic performance of 3D-printed perforated panels combined with polyurethane foam, International Journal on Interactive Design and Manufacturing (IJIDeM), https://doi.org/10.1007/s12008-024-017880-0

[57] Dussault, A., Pitaru, A. A., Weber, M. H., Haglund, L., Rosenzweig, D. H., & Villemure, I. (2022). Optimizing design parameters of PLA 3D-Printed scaffolds for bone defect repair. Surgeries, 3(3), 162–174. https://doi.org/10.3390/surgeries3030018

Author Biography

Akshay S Karad

Akshay S. Karad is presently working as Research Associate in the Department of Mechanical Engineering at Dr Vishwanath Karad MIT World Peace University (MITWPU), Pune. He did his post-graduation in Mechanical Engg from Dr Vishwanath Karad MIT World Peace University (MITWPU), Pune in 2023 and has an experience of one year at Defence Institute Advanced Technology (DIAT), Pune. He has published three research article in SCOUPS.

Mobile No.: +91 7448199359:
Linked In: www.linkedin.com/in/akshay-karad
Google Scholar: https://scholar.google.co.in/citations?user=UKJvXzEAAAAJ&hl=en
Scopus: https://www.scopus.com/authid/detail.uri?authorId=56336321200
Orcid: https://orcid.org/0000-0003-1469-3218

Dr. Ratnakar R. Ghorpade

Ratnakar R. Ghorpade is currently serving as Associate Professor in the Department of Mechanical Engineering at Dr Vishwanath Karad MIT World Peace University (MITWPU), Pune. He did his post graduate in Mechanical Engg from VIT Pune in 2003 and PhD in Mechanical Engg from SPPU, Pune in 2017. He has been engaged in teaching & Research from last 22 years. His teaching experience spans more than 22 years, Research experience is about 5 years and industrial experience is 2 years. Total 70+ publications are at his credit in National/International Journals and conferences along with 2 patents. He has authored books in his field of interest as **TRIBOLOGY (2005), ROBOTICS (2007), Strength of Machine Elements**: Concepts & Applications (2011), **Mechanical System Design (2017), Design of Machine Elements-I (2018), Design of Machine Elements-II (2018) and Theory of Machines-II (2019).** He is recognized PhD guide (w.e.f. 2018) of this university and currently guiding 6 PhD candidates, and guided 22 PG Thesis and adjudicated many of other universities. He is Life member of various society's including ISTE.

Mobile No.: +91 9370032718
Personal Web: https://sites.google.com/mitwpu.edu.in/drratnakarghorpade/
Linked In: https://in.linkedin.com/in/dr-ratnakar-r-ghorpade-429a9436
Google Scholar: **https://scholar.google.co.in/citations?user=3egailoAAAAJ&hl=en**
Scopus: https://www.scopus.com/authid/detail.uri?authorId=56336321200
Orcid: http://orcid.org/0000-0001-6540-6237
Web of Science Researcher ID: AAI-1837-2021
Vidwan Inflibnet: https://vidwan.inflibnet.ac.in/profile/146921

Dr. Puskaraj D Sonawwanay

	Dr Puskaraj D Sonawwanay is an accomplished researcher and faculty member with a diverse range of experience in mechanical engineering, including teaching, research, and administration. Dr. Sonawwanay serves as the PG Program Coordinator - Mechanical Design Engineering at Department of Mechanical Engineering, Dr. Vishwanath Karad MIT World Peace University, Pune, India. Dr Sonawwanay's research interests are focused on Materials Processing, Mechanical Engineering Design. He has to his credit 6 granted patents and 3 published patents. He has published 50 research papers in peer-reviewed international journals, international and national conferences, and co-authored 3 books and 9 book chapters. Dr Sonawwanay's work has been recognized with the prestigious 'Gandhian Young Technological Innovation (GYTI) Award 2016' by the Department of Science and Technology (DST), Government of India, at Rashtrapati Bhavan, New Delhi. The award-winning innovation is on the Design of Innovative Retrofitted Tricycle for a Disabled Person. The award is under the category of 'More from Less for Many' (MLM). He can be reached at: Email: puskarajdsonawwanay@gmail.com Website: https://puskarajdsonawwanay.com

Dr. Shivprakash B. Barve

	**Dr. Shivprakash B. Barve** is currently serving as Professor and Program Director in the Department of Mechanical Engineering at Dr Vishwanath Karad MIT World Peace University (MITWPU), Pune. He did his post graduate in Mechanical Engg. from Shivaji University, Kolhapur in 2002 and PhD in Mechanical Engg. from Shivaji University, Kolhapur, in 2008. He has been engaged in Teaching & Research from last 25 years. His Teaching and Research experience durations more than 25 years. Industrial experience is 2 years. Total 130+ publications are at his credit in National/International Journals and conferences along with 1 patent from south Africa. He has authored 3 books. He is recognized PhD and M.E/M.Tech guide of this university. **Two Ph. D. scholars completed Ph. D. under his guidance. He is** guiding 6 Ph.D. scholars, and guided 20 PG Thesis and adjudicated many of other universities. He Received research grant **Rs. 24.90 Lakhs (Twenty-Four Lakhs and Ninety Thousand only)** for Research proposal entitled “**Development and Delivery of Aero elasticity Software of Spinning Projectiles**” sanctioned by **ARMAMENT RESEARCH BOARD, Ministry of Defense,** New Delhi through **Armament Research & Development Establishment** (**ARDE**) **Pune, 2017.** He is Professional member of various society’s including IE, LMISTE, SM-IIIE, AM-IET. He can be reached at, Mobile No.: 7038894910 E-mail Id.: shivprakash.barve@mitwpu.edu.in